

# Decision-Oriented Modeling of Thermal Dynamics within Buildings

Xueyuan Cui, *Graduate Student Member, IEEE*, Jean-François Toubeau, *Member, IEEE*, François Vallée, *Member, IEEE*, and Yi Wang, *Senior Member, IEEE*

**Abstract**—To enhance the quality of energy management tasks, accurately representing the thermal dynamics of buildings is crucial. Traditional methods aim to improve the building model in regards to an arbitrary statistical metric, before feeding the trained model to the optimization-based energy management process. In this paper, we advocate for a more integrated approach, consisting of incorporating the downstream optimization directly into the training pipeline. The goal is to improve the building model in strategic operating zones, where the greatest impact on decision-making will be achieved. To that end, we first formulate the thermal dynamics as ordinary differential equations (ODEs) using neural networks. The model parameters are then updated through an end-to-end gradient-based training strategy wherein the downstream optimization is used as the loss function. To increase the robustness of the approach, the proposed loss is combined with traditional physics-informed accuracy-oriented training, employing a novel coordinated gradient descent algorithm. Simulation results show the effectiveness of the proposed modeling method, regarding both the optimality of decisions and their physical interpretability.

**Index Terms**—Building energy management, thermal dynamics, thermostatically controlled loads, neural dynamic equations.

## I. INTRODUCTION

THE building sector is responsible for more than 30% of the worldwide energy consumption, making it a key player in the transition towards low-carbon energy systems [1], [2]. Among the various building load types, Thermostatically Controlled Loads (TCLs) contribute a major proportion of energy consumption in building sectors. Simultaneously, TCLs have a strong potential for improving building energy management due to their ability to provide thermal flexibility [3]. However, to accurately dispatch TCLs for controlling the temperature within multi-zone buildings, it is necessary to properly capture the internal thermal dynamics.

When extracting the flexible regulation potential of TCLs, one basic requirement is to formulate a thermal dynamics

The work was supported in part by the National Key R&D Program of China under Grant 2022YFE0141200, in part by the Research Grants Council of the Hong Kong SAR under Grant HKU27203723, and in part by the Guangdong Basic and Applied Basic Research Foundation under Grant 2024A1515011266. (*Corresponding author: Yi Wang*)

Xueyuan Cui and Yi Wang are with the Department of Electrical and Electronic Engineering, The University of Hong Kong, Hong Kong SAR, China, and are also with The University of Hong Kong Shenzhen Institute of Research and Innovation, Shenzhen, 518057, China. (xycui@eee.hku.hk, yiwang@eee.hku.hk)

Jean-François Toubeau and François Vallée are with the Power Systems and Markets Research Group, Electrical Power Engineering Unit, University of Mons, 7000 Mons, Belgium (email: Jean-Francois.TOUBEAU@umons.ac.be, francois.vallee@umons.ac.be).

model to learn the influence relationships of electrical power to the temperature variation. It provides a basis for setting temperature control conditions and evaluating corresponding power consumption requirements. The modeling of thermal dynamics further formulates the optimization problem (e.g., model predictive control [4]) to solve the optimal temperature control decisions for various control purposes. Two main types of models can be found in the literature, i.e., physics-based and data-driven perspectives. The physics-based models rely on detailed building parameters (e.g., wall materials, window types, and zone numbers) and try to analytically recover the actual thermal dynamic process [5]. These white-box models are used by specific software (e.g., Energyplus [6] and TRN-SYS [7]) to simulate the time-varying indoor temperatures in regards to external input conditions. In general, the physical-based model achieves the highest accuracy, but their complicated model structure requires substantial building details, which makes them impractical in usual energy management applications. On the contrary, data-driven models often require little domain knowledge to represent the thermal dynamics process. Such models are typically parametrized through a supervised learning approach aiming at fitting the available measurement data [8] using arbitrary statistical metrics. These data-driven model architectures are flexible, such that the complexity level can be easily adapted based on the user's requirements, from linear (e.g., autoregressive models [9]) to nonlinear (e.g., neural networks [10]) functions. Generally, the nonlinear model with higher complexity can better represent the actual thermal dynamics. However, its black-box nature is less interpretable, which prevents quantifying the influence of explanatory factors on thermal dynamics, making it unsuitable for energy control and operation.

A more promising perspective is thus to combine the strengths of both physics-based and data-driven approaches. This can be achieved by integrating physical knowledge within the data-driven model, giving rise to grey-box models [11]. As a widely adopted solution, the resistor-capacitor (RC) circuit model gained much attention. Different RC topologies can be envisioned, and are based on a physics-based backbone structure, wherein inner parameters are identified using a data-driven process. In [12], the resistance and capacitance were used to represent the physical characteristics such as thermal conduction and inertia, and the temperature was then a circuit node variable. In [13], a more detailed model relying on lumped heat transfer coefficient, air exchange rate, and zone air heat capacity was parametrized by the least squares method with simulated data. However, all those RC models can only

capture linear dynamics, which restricts the model's accuracy. This limitation is exacerbated in multi-zone buildings with more interconnected and complex explanatory factors [14].

To improve the grey model's accuracy, Physics-informed Neural Networks (PiNNs) are increasingly adopted as new backbone structures to capture nonlinear issues [15]–[19]. In this setting, physical knowledge is inserted to improve the model's interpretability. A review of physics-informed learning was conducted in [15], where various approaches to adapt the NN architecture were shown to automatically satisfy physical properties. Specifically, two variants of PiNNs were proposed in [16], where input variables were encoded as latent components in new physics-informed loss functions. Furthermore, to explicitly express the known physical link between input variables and the thermal dynamics, inequality constraints were derived from thermal stability characteristics in [17], [18], such that the trained grey-box model can naturally comply with physical properties.

The inherent errors when modeling the thermal dynamics of buildings cause undesired (and unpredictable) deviations from the optimal decisions in the energy management process [19]. Most of the above data-driven modeling methods focused on how to improve statistical accuracy compared with true observed data, e.g., they adopted the Mean Squared Error (MSE) between the predicted and the true observed data as the training loss function. However, the practical application function of the trained model is always to formulate the downstream optimization-based energy management task to acquire optimal decisions for temperature control. There exists a high uncertainty on the impact of inherent model errors on the solution accuracy. In particular, models with even the same MSE could lead to very different optimization costs. This insight paves the way for new research aiming to integrate downstream optimization within the learning task, so as to learn a model of thermal dynamics that will yield the best decisions rather than minimizing an arbitrary, value-agnostic statistical metric.

Such a paradigm has recently emerged for solving forecasting tasks [20]–[23]. Given the ground truth results from optimization (using the actual ex-post observations of predicted variables), the relationship between forecasting errors and decision errors can be established. This mapping can then be leveraged to update the forecaster's parameters. In power load forecasting research, this mapping was approximated into a piecewise linear loss function in [20] and formulated as an end-to-end multi-objective problem in [21]. Similarly, a regression tree model and boosting method were proposed in [22] to capture the non-quadratic and asymmetric link between wind power forecasting and the costs of the downstream participation to electricity markets. Research in solar generation forecasting [23] regarded the mapping function as asymmetric perturbations to the symmetric MSE, within a traditional gradient-based learning procedure. However, although finding the ground truth model is straightforward for forecasting tasks (since only the true observation needs to be integrated into the optimization), it is very difficult in the context of modeling (partially) unknown dynamics. Indeed, it requires to embed the true building model into the optimization, which is impractical.

When integrating the downstream optimization task in the modeling procedure, another important challenge is the compatibility of time intervals. In existing modeling approaches, the time interval is determined by the measurement data. Hence, when the optimization needs to be solved with a different time granularity, resampling techniques, which are subject to information loss, need to be used. Alternatively, dynamic equation-based models can represent the continuous temperature dynamics, such that arbitrary time intervals can be derived without requiring any resampling or retraining process. A recent advancement in this realm is the Neural Ordinary Differential Equation (NODE) method [24], which enables to extract dynamic equations using neural networks. This architecture has been applied in [25], [26], yielding promising outcomes to represent diverse thermal dynamics. In this work, we will thus adopt this novel NODE-based backbone model to represent the thermal dynamics of buildings.

In light of the above context, two research questions are of particular relevance: 1) how to integrate the downstream optimization model within the learning procedure of the thermal dynamics of buildings, in the absence of a ground truth solution? 2) how to convert the output of the NODE-based approach to make it compatible with discrete-time optimization problems? To solve both problems, we propose a general training strategy by incorporating downstream optimization tasks. The proposed strategy can be widely used to train task-specific models for various downstream task types. In particular, this paper makes the following novel contributions:

- 1) **New perspective:** We couple modeling and optimization tasks in an end-to-end gradient-based training framework and then apply it to learn the thermal dynamics of multi-zone buildings. First, a NODE-based model is formulated to represent the continuous thermal dynamics, which are then leveraged by an optimization-based energy management strategy. Second, the gradients of the optimization objective over parameters of the NODE-based model are derived, which is achieved by using the implicit function theorem.
- 2) **New method:** We augment the above decision-related gradient with a physics-informed gradient that is computed using a conventional loss function. A coordinated algorithm is then proposed to generate the combined gradient adaptively, with the objective of updating model parameters to minimize optimization costs while enforcing accuracy requirements and physical interpretability.
- 3) **New finding:** We verify through case study simulations that the operation costs can be reduced with respect to traditional training approaches. We moreover demonstrate that the trade-off between costs arising from power consumption and temperature violation can be effectively controlled while maintaining the inherent physical characteristics of the building model.

The rest of this paper is organized as follows: Section II introduces the problem of properly modeling the thermal dynamics of multi-zone buildings. Section III presents the proposed decision-oriented modeling method, while Section IV explains the solution algorithm for the training process. Section V

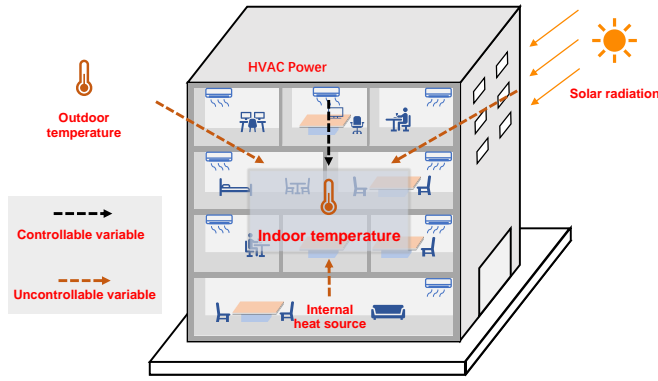


Fig. 1. Influence factors for building thermal dynamics.

conducts case studies, while Section VI draws the conclusion.

## II. PROBLEM STATEMENT

The proposed work focuses on the building temperature control scenario, where thermal dynamics modeling is first obtained and formulated into building optimization problems to solve the optimal decisions. Representing the thermal dynamics of buildings mainly amounts to capturing the variations in indoor temperature over time. As shown in Fig. 1, the indoor temperature is affected by both controllable and uncontrollable variables. Under cooling scenarios, the temperature  $\tau_i(t)$  of each individual zone  $i$  at time  $t$  is controlled by the cooling power  $q_i(t)$ . Besides, it is also influenced by exogenous factors, including the outdoor temperature  $\tau^{\text{out}}(t)$  (through exterior walls and windows), solar radiation  $q_i^{\text{rad}}(t)$  (through windows), and internal heat sources  $q_i^{\text{occ}}(t)$  (through the air and interior walls). Modeling the thermal dynamics can be presented as:

$$\dot{\tau}_i = \mathcal{M}(\mathbf{X}_i; \psi) \quad (1)$$

where  $\mathcal{M}$  is the Ordinary Differential Equation (ODE)-based model,  $\mathbf{X}_i = [\tau_i, q_i, \tau^{\text{out}}, q_i^{\text{rad}}, q_i^{\text{occ}}]$  is the input vector including all the explanatory factors, and  $\psi$  is the vector of the parameters of model  $\mathcal{M}$ .

In the existing research, the modeling stage and the downstream energy management process are always independently (and sequentially) carried out, which can be formulated as:

$$\min_{\mathbf{v}} C^{\text{opt}}(\mathbf{v} \in \mathcal{V}; \mathcal{M}(\mathbf{X}_i; \hat{\psi})) \quad (2a)$$

$$\text{s.t. } \hat{\psi} \in \arg \min_{\psi} \|\tau_i - \tilde{\tau}_i\|_2^2 + \varepsilon \quad (2b)$$

where (2a) aims at minimizing the costs of the energy management problem  $C^{\text{opt}}$ , using the trained model from (2b);  $\mathbf{v}$  is the vector of decision variables included in the feasible set  $\mathcal{V}$ ,  $\hat{\psi}$  is the vector of model parameters (e.g., weights of neural networks) which is trained by minimizing a statistical loss function with the true label data  $\tilde{\tau}_i$ , and  $\varepsilon$  is the inherent model error after training.

In the above Modeling-Then-Optimize (MTO) pattern, the model accuracy is not always consistent with the downstream optimization performance on temperature regulation. Such a

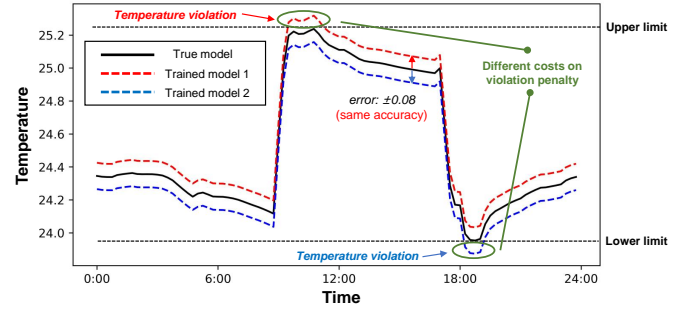


Fig. 2. Relationship between model accuracy and operation costs.

situation is depicted in Fig. 2. The model accuracy is measured by the statistical error between the predicted temperature data and the true observations. It is assumed that two different trained models have the same errors (one is always positive and the other one is negative). It can be seen that the same error can result in different optimization costs, because of asymmetries in the true cost function and penalties on the temperature violations in real cases. It reflects that traditional training strategies that purely rely on accuracy metrics cannot obtain an ideal model due to their inability to avoid costly operating zones. Therefore, it inspires us to consider how to learn a model that can reduce the optimization costs in the downstream application process.

Based on the above analysis, the training strategy of data-driven models can be enhanced, by integrating the optimization problem in model training to fully account for the downstream energy management costs. Compared with (2), the problem can be represented as:

$$\min_{\mathbf{v} \in \mathcal{V}, \psi} C^{\text{opt}}(\mathbf{v}; \mathcal{M}(\mathbf{X}_i; \psi)) \quad (3)$$

## III. DECISION-ORIENTED MODELING FRAMEWORK

The proposed decision-oriented modeling framework is presented in Fig. 3. The backbone model structure  $\mathcal{M}$  is first determined. The model training consists of a gradient-based minimization of a loss function. Here, two different losses are considered, i.e., the proposed optimization-oriented loss, which is augmented with an auxiliary accuracy-oriented loss dedicated to maintaining the known physics characteristics. All key contributions are introduced in the following subsections.

### A. Backbone Model Structure

To reduce the complexity of energy management in multi-zone buildings, we formulate the equivalent indoor temperature  $\tau(t)$  from all zones for simplification [9]. The energy conservation equation is presented as:

$$C^{\text{air}} \sum_{i \in \mathcal{Z}} c_i^{\text{mass}} \tau_i(t) = C^{\text{air}} \sum_{i \in \mathcal{Z}} c_i^{\text{mass}} \tau(t) \quad (4)$$

where  $\mathcal{Z}$  is the set of all zones  $i$  in the building;  $C^{\text{air}}$  is the specific capacity of air;  $c_i^{\text{mass}}$  is the air mass of zone  $i$ .

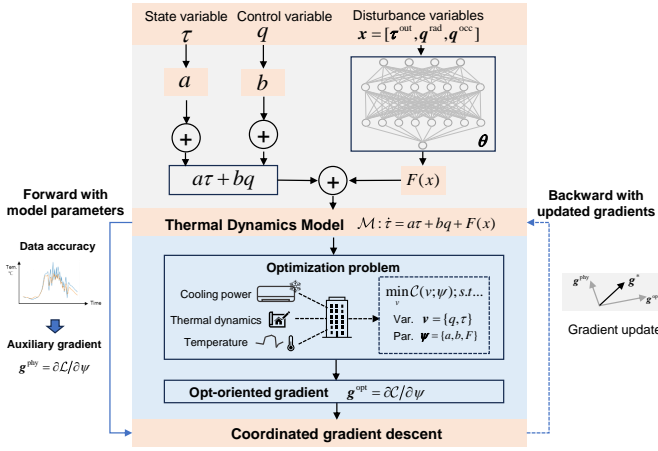


Fig. 3. Proposed decision-oriented modeling framework.

Then,  $\tau(t)$  can be derived from individual  $\tau_i(t)$  as:

$$\tau(t) = \sum_{i \in \mathcal{Z}} \zeta_i \tau_i(t), \quad \zeta_i = \frac{c_i^{\text{mass}}}{\sum_{i \in \mathcal{Z}} c_i^{\text{mass}}} \quad (5)$$

where  $\zeta_i$  is the ratio of the volume of zone  $i$  to the total volume of all zones.

We propose to control the building-level cooling power as  $q(t) = \sum_{i \in \mathcal{Z}} q_i(t)$ , while the vector of aggregated disturbance variables is defined as  $\mathbf{x}(t) = [\tau^{\text{out}}(t), q_i^{\text{rad}}(t), q_i^{\text{occ}}(t)]$ ,  $i \in \mathcal{Z}$ . Inspired from [17], the backbone model is formulated as:

$$\mathcal{M}: \dot{\tau} = a \cdot \tau + b \cdot q + F(\mathbf{x}) \quad (6)$$

where  $a$  and  $b$  are parameters for the linearized building envelope dynamics;  $F(\mathbf{x})$  represents the nonlinear disturbance dynamics, which are here extracted from Neural Networks (NNs), i.e.,  $F(\mathbf{x}) = \Psi(\mathbf{x}; \boldsymbol{\theta})$  where  $\Psi$  is the NN structure and  $\boldsymbol{\theta}$  is the vector of weight parameters.

It can be seen that the research aim is to build a surrogate model for the real-world building's thermal dynamics so that we can incorporate it into the energy management and optimization process. The model training task is to identify all the required parameters  $[a, b, \boldsymbol{\theta}]$  to determine the final model. Specifically, the model structure has a linear combination of controllable decision variables (i.e.,  $\tau$  and  $q$ ) and leaves the uncontrollable inputs  $\mathbf{x}$  in a black-box style. The advantage is that it can be utilized to formulate linear programming and reserve representation accuracy by capturing complex and coupling influences of all disturbance features.

The model  $\mathcal{M}$  is solved through a NODE-based training strategy [24], i.e., the output of  $\mathcal{M}$  at each time  $t$  is  $\dot{\tau}(t) = \frac{d\tau}{dt}$ . To infer the time series of indoor temperatures, the Euler formulation is adopted. Given the integration step  $\Delta t$ , the temperature  $\tau$  is represented as:

$$\tau(0) = \tilde{\tau}(0) \quad (7a)$$

$$\tau(t + \Delta t) = \tau(t) + \Delta t \cdot \dot{\tau}(t) \quad (7b)$$

The Euler formulation can achieve good calculation accuracy, especially with small time intervals. Note that the

proposed model structure can be seamlessly incorporated with all other feasible numerical calculation methods (e.g., Runge-Kutta).

The temperature at each time step  $t$  of the training period  $\mathcal{T}$  can then be derived as:

$$\tau(t + \Delta T) = \tau(t) + \Delta t \cdot \sum_{n=0}^{N-1} \dot{\tau}(t + n \cdot \Delta t), \quad \forall t \in \mathcal{T} \quad (8)$$

where  $\Delta T$  is the time interval of the collected data. The integration step  $\Delta t$  is selected such that the collected data satisfy the required time intervals  $\Delta T = N \cdot \Delta t$  with  $N$  steps.

*Discussion:* We compare the proposed model structure with the commonly used RC-based modeling approach [11] to explain the application scenarios. While RC models require detailed physical property parameters (e.g., heat capacity, heat absorption coefficient, and air mass flow) to calculate parameters in the linear equation, the proposed model requires measured data of all input variables and corresponding temperature curves to identify model parameters in a data-driven way. Besides, the accuracy of the RC model tends to be decreased due to complex and coupling thermal dynamics characteristics in multi-zone buildings, but the proposed NN-based model can ensure accuracy through its nonlinear representation ability [27].

After obtaining the temperature variables, the subsequent task is to design the training framework to update model parameters  $\boldsymbol{\psi} = [a, b, \boldsymbol{\theta}]^T$ . This is achieved using two loss functions, which are presented in subsections III-B and III-C.

## B. Optimization-oriented Loss Function

1) *Optimization problem:* The day-ahead building energy management problem aims at minimizing the costs  $\mathcal{C}^{\text{opt}}$  [28], and is expressed as:

$$\min \mathcal{C}^{\text{opt}} = \sum_{t \in \mathcal{T}} c_t p(t) + c^U e^U(t) + c^L e^L(t) \quad (9a)$$

s.t.

$$\tau(t + \Delta t) = \tau(t) + \Delta t \cdot (a\tau(t) + bq(t) + F(\mathbf{x}(t))) \quad (9b)$$

$$q(t) = \eta p(t) \quad (9c)$$

$$\underline{p} \leq p(t) \leq \bar{p} \quad (9d)$$

$$\underline{\tau}_t - e^L(t) \leq \tau(t) \leq \bar{\tau}_t + e^U(t) \quad (9e)$$

$$0 \leq e^L(t), e^U(t) \leq \bar{e} \quad (9f)$$

where  $c_t$  is the real-time electricity price at time  $t$ ;  $p(t)$  is the power magnitude of TCLs at time  $t$ ;  $e^U(t)$  and  $e^L(t)$  are the violations of upper and lower temperature constraints;  $c^U$  and  $c^L$  are the corresponding penalty coefficients for the violations;  $\eta$  is the coefficient of performance (COP) of the TCL's energy conversion;  $\underline{p}$  and  $\bar{p}$  are the minimum and maximum power limits of TCLs;  $\underline{\tau}_t$  and  $\bar{\tau}_t$  are the lower and upper limits of temperature, and  $\bar{e}$  limits the maximum tolerance of temperature violation.

The objective (9a) minimizes the energy consumption costs and the violation costs of temperature limits. Constraint (9b) determines the temperature at each time based on the trained model, while (9c) defines the linear conversion between

electrical and cooling power. Finally, constraints (9d) - (9f) regulate the range of indoor temperature variation and TCLs power output at each time step. After combining the linear objective term and other linear constraints, the proposed model structure formulates a linear programming (LP) type. The same LP problem type can be also formulated with other linear model structures.

In this problem, the decision variables  $\mathbf{v} = [q, \tau, p, e^U, e^L]^T$  are optimized based on the building's model parameters  $\boldsymbol{\psi} = [a, b, \theta]^T$ . All influence factors in  $\mathbf{x}(t)$  are obtained from a day-ahead forecasting task and are regarded as boundary conditions in the optimization problem. We assume them with perfect forecasting and recognize the potential influence of forecasting errors in future decision-oriented research.

2) *Gradient derivation*: To ensure that the proposed approach minimizes energy management costs, the optimization objective  $\mathcal{C}^{\text{opt}}$  is taken as the loss function to train the model  $\mathcal{M}$  of thermal dynamics. This procedure requires to compute the gradient of the objective  $\mathcal{C}^{\text{opt}}$  with respect to parameters  $\boldsymbol{\psi}$ . This is achieved by leveraging the optimization differentiable neural network (OptNet) proposed in [29], where the desired gradient is computed indirectly by solving Karush–Kuhn–Tucker (KKT) conditions.

Specifically, we first rewrite (9) into the general form with equality constraints  $\mathbf{f}$  and inequality constraints  $\mathbf{h}$  as

$$\min \mathcal{C}^{\text{opt}}(\mathbf{v}) \quad (10a)$$

$$\text{s.t. } \mathbf{f}(\mathbf{v}, \boldsymbol{\psi}) = 0 : (9b), (9c) \quad (10b)$$

$$\mathbf{h}(\mathbf{v}, \boldsymbol{\psi}) \leq 0 : (9e), (9f), (9d) \quad (10c)$$

Then, the Lagrangian function  $\mathcal{L}$  of the optimization problem is formulated as:

$$\mathcal{L}(\mathbf{v}, \boldsymbol{\lambda}, \boldsymbol{\mu}) = \mathcal{C}^{\text{opt}}(\mathbf{v}) + \boldsymbol{\lambda}^T \mathbf{f}(\mathbf{v}, \boldsymbol{\psi}) + \boldsymbol{\mu}^T \mathbf{h}(\mathbf{v}, \boldsymbol{\psi}) \quad (11)$$

where  $\boldsymbol{\lambda}$  and  $\boldsymbol{\mu} \geq 0$  are the dual variables corresponding to equality and inequality constraints, respectively.

If the problem in (10) is convex and continuous, the strong duality holds, and the KKT conditions are then sufficient and necessary conditions for optimality. Besides the inherent inequality constraints (10c), KKT conditions for stationarity, primal feasibility, and complementary slackness include:

$$\mathcal{K} = \begin{bmatrix} \frac{\partial \mathcal{L}(\mathbf{v}, \boldsymbol{\lambda}, \boldsymbol{\mu}; \boldsymbol{\psi})}{\partial \mathbf{v}} \\ \mathbf{f}(\mathbf{v}, \boldsymbol{\psi}) \\ \boldsymbol{\mu}^T \mathbf{h}(\mathbf{v}, \boldsymbol{\psi}) \end{bmatrix} = 0 \quad (12)$$

where  $\mathcal{K}$  is regarded as the implicit function of  $\mathbf{v}, \boldsymbol{\psi}$  for the optimality conditions of the problem.

According to the implicit function theorem [30], the derivative of  $\mathcal{K}$  with respect to  $\boldsymbol{\psi}$  exists and the following condition needs to be satisfied:

$$\frac{\partial \mathcal{K}}{\partial \boldsymbol{\psi}} + \frac{\partial \mathcal{K}}{\partial \mathbf{v}} \cdot \frac{\partial \mathbf{v}}{\partial \boldsymbol{\psi}} = 0 \quad (13)$$

from which we can derive the gradient of decision variables over model parameters as:

$$\frac{\partial \mathbf{v}}{\partial \boldsymbol{\psi}} = - \left[ \frac{\partial \mathcal{K}}{\partial \boldsymbol{\psi}} \right]^{-1} \frac{\partial \mathcal{K}}{\partial \boldsymbol{\psi}} \quad (14)$$

Finally, the desired gradients  $\mathbf{g}^{\text{opt}} = \frac{\partial \mathcal{C}^{\text{opt}}}{\partial \boldsymbol{\psi}}$  are derived from the chain rule as:

$$\mathbf{g}^{\text{opt}} = \frac{\partial \mathcal{C}^{\text{opt}}}{\partial \boldsymbol{\psi}} = \frac{\partial \mathcal{C}^{\text{opt}}}{\partial \mathbf{v}} \cdot \frac{\partial \mathbf{v}}{\partial \boldsymbol{\psi}} \quad (15)$$

where the  $\frac{\partial \mathcal{C}^{\text{opt}}}{\partial \mathbf{v}}$  can be easily derived from (9a), while  $\frac{\partial \mathbf{v}}{\partial \boldsymbol{\psi}}$  can be explicitly determined by (14).

The derived gradient  $\mathbf{g}^{\text{opt}}$  represents the change rate of the optimization objective over model parameters and is adopted to update parameters  $\boldsymbol{\psi}$  using gradient descent.

Note that we make some reasonable assumptions on optimization problem types for the straightforward gradient calculation. Firstly, we adopt convex optimization types to effectively minimize the objective costs with KKT conditions. Besides, we do not consider some specific optimization types with non-differentiable cases (e.g., linear programming with parameters to be identified in the objective function, mixed integer linear programming, etc.). Various effective approaches to tackle the above problems can be referred to in [31].

### C. Physics-informed Auxiliary Loss Function

When incorporating the proposed optimization-based gradient into the model training process, the model accuracy and compliance with physical characteristics cannot always be guaranteed. Because there is no ground-true and mathematical model to calculate the true costs with inputted decisions, there is no feedback from the true building, and it is hard to ensure an effective gradient for decision optimization. In Fig. 4, we present the variation in both model accuracy (RMSE loss) and objective value  $\mathcal{C}^{\text{opt}}$  as a function of the model parameter (taking here  $b$  as an example while keeping all other parameters in  $\boldsymbol{\psi}$  constant). It can be seen that the model  $\mathcal{M}$  is most accurate when values of  $b$  are around -0.4. In contrast, the objective value monotonically decreases when the value of  $b$  is reduced. From this, one can expect that only utilizing the optimization objective to guide the training process would lead to a convergence of  $b$  below -0.7. This outcome would largely deviate from the physical characteristics of thermal dynamics within buildings. Therefore, we propose to enrich the optimization-oriented loss with a physics-constrained function, such as to maintain the accuracy of the data-driven model.

1) *Physical characteristics*: For the ODE equation (6), the physical characteristics mainly refer to the self-stability of the thermal dynamics process and the correct relationship between indoor temperature variations and explanatory factors [17]. In the cooling scenario, the physical laws are formulated as:

$$\begin{cases} a < 0 \\ \frac{\partial \tau(t+\Delta t)}{\partial q(t)} \leq 0 \\ \frac{\partial \tau(t+\Delta t)}{\partial \tau^{\text{out}}(t)} \geq 0, \frac{\partial \tau(t+\Delta t)}{\partial q^{\text{rad}}(t)} \geq 0, \frac{\partial \tau(t+\Delta t)}{\partial q^{\text{occ}}(t)} \geq 0 \end{cases} \quad (16)$$

where the first term ensures the stability of the state variable; the second term enforces the negative correlation between indoor temperature and cooling power; while the third term represents the positive correlation between indoor temperature and all the disturbance variables.

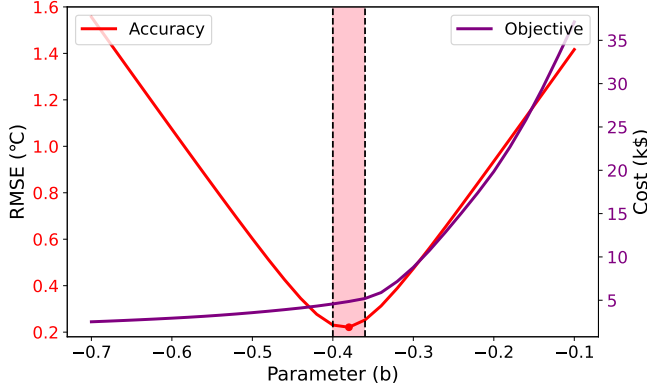


Fig. 4. Change of model accuracy and objective with parameter  $b$ .

However, the above physical laws are difficult to incorporate into model training, and we need to further transform them into explicit constraints on model parameters  $\psi$  (rather than on the temperature  $\tau$ ). To that end, we first assume that explanatory factors do not vary during a short time  $[t, t + \Delta t]$ , and we calculate the function of  $\tau(t)$  based on (6):

$$\begin{aligned} \tau(t) &= Ae^{at} - \frac{1}{a}(bq(t) + F(\mathbf{x}(t))) \\ A &= \tau(0) + \frac{1}{a}[bq(0) + F(\mathbf{x}(0))] \end{aligned} \quad (17)$$

where the parameter  $A$  is defined based on the initial condition.

By assuming that explanatory factors  $q(t), \mathbf{x}(t)$  are also constant over short intervals, we can then derive  $\tau(t + \Delta t)$ :

$$\tau(t + \Delta t) = Ae^{a(t+\Delta t)} - \frac{1}{a}[bq(t) + F(\mathbf{x}(t))] \quad (18)$$

Thus, we can determine new limits on model parameters as:

$$\begin{cases} \frac{\partial \tau(t+\Delta t)}{\partial q(t)} = -\frac{b}{a} \leq 0 \Rightarrow b \leq 0 \\ \frac{\partial \tau(t+\Delta t)}{\partial \mathbf{x}(t)} = \frac{\partial \tau(t+\Delta t)}{\partial F(\mathbf{x}(t))} \cdot \frac{\partial F(\mathbf{x}(t))}{\partial \mathbf{x}(t)} = \\ -\frac{1}{a} \cdot \frac{\partial F(\mathbf{x}(t))}{\partial \mathbf{x}(t)} \geq 0 \Rightarrow \frac{\partial F(\mathbf{x}(t))}{\partial \mathbf{x}(t)} \geq 0 \end{cases} \quad (19)$$

Overall, the derived physical constraints can be summarized as follows:

$$\begin{cases} a < 0 \\ b \leq 0 \\ \frac{\partial F}{\partial \tau_{\text{out}}} \geq 0, \frac{\partial F}{\partial q_{\text{rad}}} \geq 0, \frac{\partial F}{\partial q_{\text{occ}}} \geq 0 \end{cases} \quad (20)$$

2) *Auxiliary loss function*: After describing the physical laws governing the thermal dynamics of the building in (20), we transform these inequality constraints into penalty terms that can be enforced during the training of model  $\mathcal{M}$ :

$$\begin{cases} a \leq 0 \Rightarrow \min [a]^+ \\ b \leq 0 \Rightarrow \min [b]^+ \\ \frac{\partial F}{\partial \tau_{\text{out}}} \geq 0 \Rightarrow \min \left[-\frac{\partial F}{\partial \tau_{\text{out}}}\right]^+ \\ \frac{\partial F}{\partial q_{\text{rad}}} \geq 0 \Rightarrow \min \left[-\frac{\partial F}{\partial q_{\text{rad}}}\right]^+ \\ \frac{\partial F}{\partial q_{\text{occ}}} \geq 0 \Rightarrow \min \left[-\frac{\partial F}{\partial q_{\text{occ}}}\right]^+ \end{cases} \quad (21)$$

where  $[\cdot]^+$  is equivalent to  $\max\{\cdot, 0\}$ .

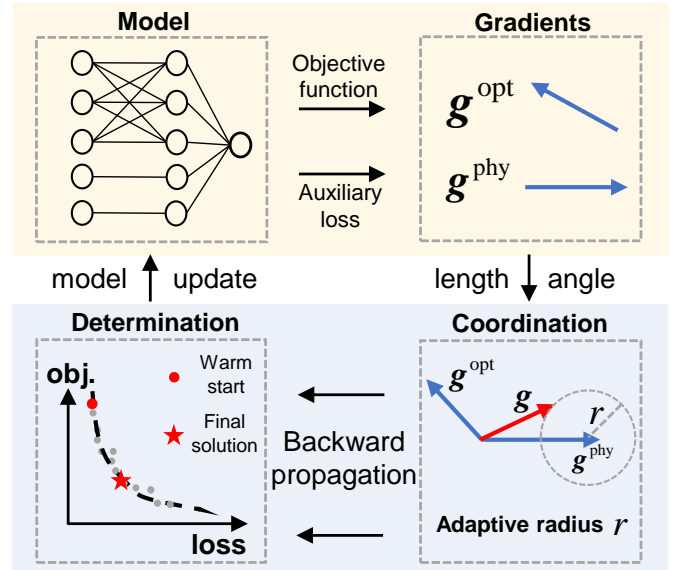


Fig. 5. Proposed algorithm for model training.

Those penalty terms can then be added to a traditional MSE-based loss, thereby giving rise to the following physics-constrained auxiliary function  $\mathcal{L}^{\text{phy}}$ :

$$\begin{aligned} \mathcal{L}^{\text{phy}}(\tau, \tilde{\tau}; \psi) &= \frac{1}{|\mathcal{T}|} \sum_{t \in \mathcal{T}} \|\tau(t) - \tilde{\tau}(t)\|_2^2 + \omega^{\text{R}} \|\mathbf{R}(t)\|_2^2 \\ \mathbf{R} &= \left[ [a]^+, [b]^+, \left[-\frac{\partial F}{\partial \tau_{\text{out}}}\right]^+, \left[-\frac{\partial F}{\partial q_{\text{rad}}}\right]^+, \left[-\frac{\partial F}{\partial q_{\text{occ}}}\right]^+ \right]^{\text{T}} \end{aligned} \quad (22)$$

where  $\tilde{\tau}(t)$  is the true temperature value from the collected dataset,  $\mathbf{R}$  is the vector containing all physical penalty terms, and  $\omega^{\text{R}}$  is the vector of corresponding penalty coefficients.

The physics-constrained auxiliary gradient is determined as  $\mathbf{g}^{\text{phy}} = \frac{\partial \mathcal{L}^{\text{phy}}}{\partial \psi}$ , which represents the change rate of the physical loss over model parameters  $\psi$ .

#### IV. COORDINATED GRADIENT DESCENT ALGORITHM

As described in Section III, two complementary loss functions are derived for guiding the model  $\mathcal{M}$  training process. The optimization-oriented loss function  $\mathcal{L}^{\text{opt}}$  teaches  $\mathcal{M}$  to minimize the costs in the energy management task, while the physical-constrained auxiliary loss function  $\mathcal{L}^{\text{phy}}$  ensures both the accuracy and physical interpretability of the trained model. On this basis, this section proposes a coordinated gradient descent algorithm to coordinate both derived gradients  $\mathbf{g}^{\text{opt}}$  and  $\mathbf{g}^{\text{phy}}$ , thereby reaching a trade-off between the optimization cost and the model's accuracy.

The algorithmic flow is depicted in Fig. 5. The main idea is to generate the combined gradient for the backward training pass based on  $\mathbf{g}^{\text{opt}}$  and  $\mathbf{g}^{\text{phy}}$ . This is achieved by generating a Pareto set between the objective cost and accuracy loss.

Coordinating both gradient vectors  $\mathbf{g}^{\text{opt}}$  and  $\mathbf{g}^{\text{phy}}$  is challenging since their directions can be contradictory, i.e.,  $\langle \mathbf{g}^{\text{phy}}, \mathbf{g}^{\text{opt}} \rangle = (\mathbf{g}^{\text{phy}})^{\text{T}} \cdot \mathbf{g}^{\text{opt}} < 0$ , so that adapting the model in the direction of one gradient can worsen the other

objective. Therefore, the proposed algorithm aims to determine a coordinated gradient vector  $\mathbf{g}$  that minimizes the conflict degree between the two gradients [32]. We express it as:

$$\max_{\mathbf{g}} \min \{ \langle \mathbf{g}^{\text{phy}}, \mathbf{g} \rangle, \langle \mathbf{g}^{\text{opt}}, \mathbf{g} \rangle \} \quad (23a)$$

$$\text{s.t. } \|\mathbf{g} - \mathbf{g}^{\text{phy}}\| \leq r \|\mathbf{g}^{\text{phy}}\| \quad (23b)$$

where  $\mathbf{g}$  is the (desired) coordinated gradient and  $r$  is the radius determining the allowable optimization space. In the objective (23a), the more contradictory gradient set (i.e., with the smaller inner product) is first selected, and the objective is then to maximize this inner product by finding the  $\mathbf{g}$ -vector that reduces contradictions. Constraint (23b) limits the search space of  $\mathbf{g}$  around  $\mathbf{g}^{\text{phy}}$  within the radius  $r$ , which can effectively ensure model accuracy during the training process.

Solving (23) is a complex task due to the high dimensionality of the gradient vector  $\mathbf{g}$ , which is equal to the number of model parameters in  $\psi = [a, b, \theta]$ . Inspired by [32], we reduce the computational burden in each optimization step by deriving the dual objective term of (23), which enables reducing the number of variables in the optimization problem.

To that end, we first define a new gradient vector  $\mathbf{g}^{\text{com}}$  as the weighted combination of gradients  $\mathbf{g}^{\text{phy}}$  and  $\mathbf{g}^{\text{opt}}$ :

$$\mathbf{g}^{\text{com}} = \omega^{\text{phy}} \mathbf{g}^{\text{phy}} + \omega^{\text{opt}} \mathbf{g}^{\text{opt}} \quad (24a)$$

$$\omega^{\text{phy}} + \omega^{\text{opt}} = 1, \omega^{\text{phy}} \geq 0, \omega^{\text{opt}} \geq 0 \quad (24b)$$

where  $\omega = [\omega^{\text{phy}}, \omega^{\text{opt}}]^T$  is the corresponding weight vector constrained by (24b). The process of finding a smaller inner product term  $\min \{ \langle \mathbf{g}^{\text{phy}}, \mathbf{g} \rangle, \langle \mathbf{g}^{\text{opt}}, \mathbf{g} \rangle \}$  in (23a) is then replaced by  $\min \langle \mathbf{g}^{\text{com}}, \mathbf{g} \rangle$  wherein  $\omega$  has to be determined.

We reformulate (23) as an unconstrained problem by adding a squared penalty term on the constraint (23b):

$$\max_{\mathbf{g}} \min_{\omega, \lambda \geq 0} (\mathbf{g}^{\text{com}})^T \mathbf{g} - \frac{\lambda}{2} (\|\mathbf{g} - \mathbf{g}^{\text{phy}}\|_2^2 - r^2 \|\mathbf{g}^{\text{phy}}\|_2^2) \quad (25)$$

The dual form is obtained by changing the max and min order as:

$$\min_{\omega, \lambda \geq 0} \max_{\mathbf{g}} (\mathbf{g}^{\text{com}})^T \mathbf{g} - \frac{\lambda}{2} (\|\mathbf{g} - \mathbf{g}^{\text{phy}}\|_2^2 - r^2 \|\mathbf{g}^{\text{phy}}\|_2^2) \quad (26)$$

To solve (26), we first determine the optimal solution  $\mathbf{g}^*$  of the inner max problem, which yields:

$$\mathbf{g}^* = \mathbf{g}^{\text{phy}} + \frac{\mathbf{g}^{\text{com}}}{\lambda} \quad (27a)$$

$$\min_{\omega, \lambda \geq 0} (\mathbf{g}^{\text{com}})^T \mathbf{g}^{\text{phy}} + \frac{\|\mathbf{g}^{\text{com}}\|_2^2}{2\lambda} + \frac{\lambda r^2 \|\mathbf{g}^{\text{phy}}\|_2^2}{2} \quad (27b)$$

Second, we solve the outer min problem to find the optimal  $\lambda^*$ -value:

$$\lambda^* = \frac{\|\mathbf{g}^{\text{com}}\|}{r \|\mathbf{g}^{\text{phy}}\|} \quad (28a)$$

$$\min_{\omega} (\mathbf{g}^{\text{com}})^T \mathbf{g}^{\text{phy}} + r \|\mathbf{g}^{\text{com}}\| \|\mathbf{g}^{\text{phy}}\| \quad (28b)$$

Finally, the optimal solution  $\mathbf{g}^{\text{com}*}$  is determined by solving the resulting problem (28b), and the coordinated gradient is derived by combining (27a) and (28a), i.e.:

$$\mathbf{g}^* = \mathbf{g}^{\text{phy}} + r \frac{\|\mathbf{g}^{\text{phy}}\|}{\|\mathbf{g}^{\text{com}*}\|} \mathbf{g}^{\text{com}*} \quad (29)$$

After obtaining the gradient  $\mathbf{g}^*$ , the model parameters are updated with a gradient descent-based training strategy. The whole training algorithm is given in Algorithm 1. In Step I, we first pre-train the model  $\mathcal{M}$  using only  $\mathbf{g}^{\text{phy}}$  to generate an accurate model, which is taken as a warm start to reduce the number of iterations of the following training process. In Step II, we determine  $\mathbf{g}_k^*$  at each  $k$ -th iteration to update the model parameters  $\psi$ . The objective values  $\mathcal{C}_k^{\text{opt}}$  and accuracy losses  $\mathcal{L}_k^{\text{phy}}$  at each iteration are stored to generate a Pareto set. In Step III, we set the tolerance range  $\epsilon$  around the accuracy of the pre-trained model (of Step I), and we determine the final model with the lowest objective value within this preset region. The error tolerance range is always preset by decision-makers. A larger  $\epsilon$  will collect more feasible points with low decision costs to determine the final model. Still, the potential risk is a larger deviation from the true operation conditions in actual buildings. The  $\epsilon$  is empirically set as 0.05-0.10, which varies from different building types and the iterative performance during the training process. Besides, we propose an adaptive radius  $r_k$  setting for better convergence in the training process (line 5), which is updated based on the vector magnitude of  $\mathbf{g}_k^{\text{phy}}$  at each iteration. In this way, the optimization-based gradient will prevail when  $\|\mathbf{g}_k^{\text{phy}}\|$  is relatively lower (i.e., when the model is already accurate), while the accuracy is strengthened when  $\|\mathbf{g}_k^{\text{phy}}\|$  becomes larger than the initial vector magnitude  $\mathbf{g}_0^{\text{phy}}$ . The sufficiency of generating a candidate set is mainly ensured by the adaptive adjustment of radius  $r$  to obtain ideal models that achieve lower decision costs given the required accuracy range. The radius  $r$  is adaptively updated by the magnitude of gradient  $\mathbf{g}_k^{\text{phy}}$  at each iteration  $k$  without the need for an artificial setting.

Based on the proposed training algorithm, our training purpose becomes “minimizing optimization costs with the trained model, but within the required accuracy range”, where the accuracy range ensures that the trained model corresponds to the actual operation of the true building. Ideally, the trained model can represent the true behavior of the actual building given the accuracy range, while we minimize the optimization costs with the trained model simultaneously. Those two conditions help ensure the finalized solution yields a better optimization performance in actual buildings.

## V. CASE STUDIES

In the case studies, we verify the performance of the proposed decision-oriented modeling method. We investigate the optimization costs, model accuracy, and algorithm performance compared with traditional Modeling-Then-Optimize (MTO) based solutions. Furthermore, scalability and robustness analysis in larger buildings are also evaluated. We finally discuss the implementation details of the proposed method in the real world. Source code, input data, and the trained details are available on Github<sup>1</sup>.

### A. Simulation Setup

1) *Data preparation*: To verify the effectiveness of the proposed methods, we utilize different building prototypes

<sup>1</sup><https://github.com/hkuedl/Decision-Oriented-Thermal-Dynamics-Modeling>

### Algorithm 1 Coordinated Gradient Descent Algorithm

**Input:** Initial model parameter vector  $\psi_0$ ; differentiable loss functions  $\mathcal{L}^{\text{opt}}$  and  $\mathcal{L}^{\text{phy}}$ ; initial constant  $r_0 \in [0, 1)$ ; maximum epochs  $K$ ; accuracy loss threshold  $\epsilon$ .

**Output:** The thermal dynamics model after training:  $\hat{\tau} = \tilde{a}\tau + \tilde{b}q + \tilde{F}(\mathbf{x})$ , where  $\tilde{F}(\mathbf{x}) = \Psi(\mathbf{x}; \tilde{\theta})$ .

#### STEP I: Model pre-train

- 1: Train the model with loss function  $\mathcal{L}^{\text{phy}}$  based on back-propagation strategy, where the required data types involve all the input features  $[q(t), \tau^{\text{out}}(t), q^{\text{rad}}(t), q^{\text{occ}}(t)]$  and corresponding labels  $\tau(t)$ ;
- 2: Calculate gradients  $\mathbf{g}_0^{\text{phy}}$  and  $\mathbf{g}_0^{\text{opt}}$  of the warm start model;

#### STEP II: Pareto set generation

- 3: **for**  $k = 1, 2, \dots, K$  **do**
- 4: Obtain normalized gradients

$$\bar{\mathbf{g}}_k^{\text{phy}} = \frac{\mathbf{g}_k^{\text{phy}}}{\|\mathbf{g}_k^{\text{phy}}\|}, \quad \bar{\mathbf{g}}_k^{\text{opt}} = \frac{\mathbf{g}_k^{\text{opt}}}{\|\mathbf{g}_k^{\text{opt}}\|}; \quad (30)$$

- 5: Update radius adaptively:  $r_k = \frac{2}{1 - e^{-\|\mathbf{g}_0^{\text{phy}}\| / \|\mathbf{g}_k^{\text{phy}}\|}} - 1$ ;
- 6: Solve optimal  $\omega_k^*$  by (28b) and  $\mathbf{g}_k^{\text{com}^*}$  by (24a);
- 7: Determine the optimal gradient vector by (29);
- 8: Update model parameters with the gradient descent algorithm as

$$\psi_{k+1} = \psi_k - \alpha \mathbf{g}_k^* \quad (31)$$

where  $\alpha$  is the learning rate;

- 9: Calculate gradients  $\mathbf{g}_{k+1}^{\text{phy}}$  and  $\mathbf{g}_{k+1}^{\text{opt}}$  for next epoch;
- 10: **end for**
- 11: Generate the Pareto set  $\mathbb{P}$  after training with  $K$  epochs as

$$\mathbb{P} = \{(\mathcal{L}_k^{\text{phy}}, \mathcal{C}_k^{\text{opt}}), k = 0, 1, 2, \dots, K\} \quad (32)$$

#### STEP III: Model determination

- 12: Find the optimal index  $\tilde{k}$  in the Pareto set by solving

$$\min_k \left\{ \mathcal{C}_k^{\text{opt}} \mid \text{s.t.} \left| \frac{\mathcal{L}_k^{\text{phy}} - \mathcal{L}_0^{\text{phy}}}{\mathcal{L}_0^{\text{phy}}} \right| \leq \epsilon, (\mathcal{L}_k^{\text{phy}}, \mathcal{C}_k^{\text{opt}}) \in \mathbb{P} \right\} \quad (33)$$

- 13: Obtain the final model with parameters  $\psi_{\tilde{k}} = [\tilde{a}, \tilde{b}, \tilde{\theta}]$ .

from the U.S. Department of Energy (DOE) for case simulation. The primarily selected building types include a 6-zone residential house, a 10-zone mall, and an 18-zone medium office. Then a 67-zone hotel and a 90-zone apartment are also utilized for scalability analysis. The historical operation data are all simulated with the Energyplus software [33], and the simulation period is set from 1st June to 31st August. The available data include the indoor temperature in each zone ( $^{\circ}\text{C}$ ), outdoor temperature ( $^{\circ}\text{C}$ ), solar radiation power (kW), internal occupant power (kW), and HVAC cooling power (kW) of all zones. The time granularity of data is 15 min. The equivalent indoor temperature of the building is calculated using (5).

2) *Simulation settings:* The simulation period is split into the training period (01/06-31/07) and the test period (01/08-31/08). To facilitate the Euler-based ODE training process and calculate the indoor temperature value at each time

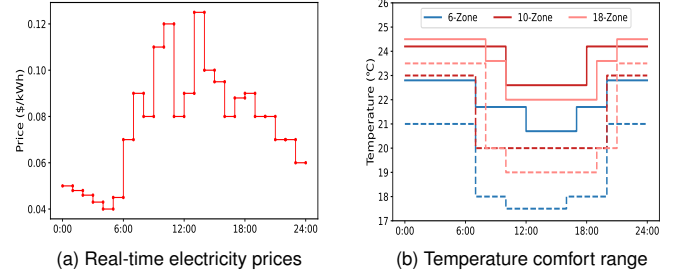


Fig. 6. Input data of daily electricity prices and comfort ranges.

TABLE I  
PARAMETER SETTINGS IN THE PROPOSED METHOD

	Parameter	Value	Parameter	Value
Model	hidden layers	3	$\eta$	3.6
	hidden units	48	$\underline{p}, \bar{p}$	0, 60 (kW)
	activation	ReLU	$c^L$	0.5 ( $^{\circ}\text{C}$ )
	optimizer	Adam	$c^U$	0.8 ( $^{\circ}\text{C}$ )
	batch size	16	$\bar{\epsilon}$	0.5 ( $^{\circ}\text{C}$ )
	/	/	$\omega^R$	5.0
Algorithm	$K$	30	$\epsilon$	0.05-0.10

step, the integration step  $\Delta t$  is fixed at 15 min. In the proposed Algorithm 1, equation (31) adopts a decay strategy for adapting the learning rate  $\alpha$  for better convergence. Key parameters in both the NODE-based model structure and the optimization problem are presented in Table I. The real-time price signals [34] and temperature comfort ranges [35] are both shown in Fig. 6. The peak period of the electricity price mainly occurs in the 9:00-14:00 interval, while the valley periods typically cover the 0:00-6:00 and 21:00-24:00 intervals. The comfort range for the indoor temperature is set differently for each building, depending on its function (e.g., office versus house). Python libraries including PyTorch [36], torchdiffeq [37], and cvxpylayers [38] are used for NN modeling, ODE model training, and optimization-oriented gradient calculation, respectively. All algorithms are executed on a computer with a 3.40 GHz Intel Xeon(R) CPU with 16 GB of RAM.

### B. Evaluation of Operation Costs

In the proposed training process of  $\mathcal{M}$ , the optimization problem in (9) needs to be formulated and solved for each training day. After obtaining the final model  $\mathcal{M}$  of the thermal dynamics of the building, its performance can be evaluated on the test set. To that end, the trained building model  $\mathcal{M}$  is fed to the optimization, and the optimal daily decisions regarding both cooling power and indoor temperature schedules can then be determined using commercial solvers.

Besides, we propose two typical modeling methods for comparison. One is the mentioned ‘‘RC Model’’ in Subsection III.A, whose model structure is linear and the parameters are identified through historical data. Another one is the ‘‘MTO’’ method that uses the same model structure as the proposed work but with only  $\mathcal{L}^{\text{phy}}$  as the training loss function.

When evaluating the optimization costs of all modeling methods, the outcomes are biased by the fact that the optimization is guided by an approximated model of the true

building. To quantify the actual ex-post operation performance of the model, the obtained schedule for indoor temperatures is thus fed into the Energyplus software, and the corresponding cooling power outcomes are determined. This cooling pattern can be regarded as the actual power consumption from the real building. All objective values in the case study are set as simulation results.

Based on these simulated results, we present the different cost terms in Table II, where “Power” and “Tem” respectively refer to the power consumption and the penalty for temperature violations in the objective (9a), while the “Sum” represents the aggregated objective value.

Compared with the regular MTO approach, the operation costs of the proposed method are significantly reduced for all types of buildings. The total costs in the training period are reduced by 9.11%, 0.57%, and 0.11% in 6-zone, 10-zone, and 18-zone buildings, respectively. Similar cost reductions are observed in the test set. We observe that the cost reductions slightly vary among buildings. Interestingly, we observe that the costs are mainly reduced in the term corresponding to temperature violations. This means that the proposed decision-oriented training learns to avoid the operating schedules leading to expensive violations of comfort constraints. For the 10-zone building, there is a 3.02% reduction of the temperature violation costs while a 0.05% reduction is achieved for the costs associated with power consumption. A more striking case is the 6-zone building, where a 43.59% cost reduction is achieved by reducing the temperature violations, while gains of only 0.01% could be reaped by improving the power consumption schedule. Such observations can be explained by the fact that the temperature violation is affected by all factors, while the power consumption is mainly caused by the cooling power factor. During the training process, the temperature violation part has thus a larger improvement space.

Similarly, the proposed method achieves lower costs compared with the RC model method in all building cases. The cost reduction level is generally larger in the temperature violation part than power consumption, which also shows higher improvement potential in reducing temperature violation of decision-oriented learning. As for the comparison between the RC model and MTO, it can be seen that the RC model achieves lower costs in the 6-zone building but higher costs in both 10-zone and 18-zone cases. Different surrogate model structures between the RC model and the proposed one result in different decisions in building energy optimization. Because both the RC model and MTO ignore downstream optimization tasks during the training period, the influences of modeling results on the optimization problem are uncertain. Still, they both achieve higher decision costs than the proposed work.

Furthermore, we represent the probability distribution of the daily cost difference between the proposed method and MTO, RC model, respectively in Fig. 7. Positive values mean that the proposed method leads to higher costs, while negative values correspond to better decisions from the proposed method. We see that the daily cost performance is different for each building. When compared with the MTO method in Fig. 7a, the daily cost difference is mainly distributed around 0 and -1 in the 6-zone building. However, the longer tail in negative

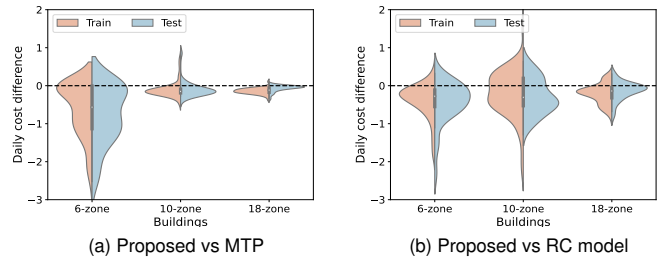


Fig. 7. Daily cost error distributions in training and test sets.

values indicates that several days in both the training and test periods have a strong potential for cost reductions. These extreme days contribute to the major part of the total cost reductions. The cost difference of the 10-zone building is smoothly distributed around -0.2, indicating that the proposed method regularly outperforms the MTO approach in both training and test sets. In the 18-zone building, the proposed method is also consistently better, but there is a mismatch between the training and test sets, where larger cost reductions are generated in the training period.

### C. Statistical Accuracy of the Building Model

The model  $\mathcal{M}$  is evaluated in this part to ensure that both the accuracy and the physical characteristics are well captured, which is essential to provide robustness guarantees to human operators.

First, we adopt widely-used statistical metrics, including root mean square error (RMSE), mean absolute error (MAE), and R2, to evaluate the accuracy in both the training and the test dataset [14]. The outcomes are shown in Table III. Among the three comparison methods, the RC model always achieves the largest error values compared with the proposed model. The major reason is that the purely linear model can hardly capture the underlying nonlinear influence of multiple influence factors. This disadvantage is magnified in larger buildings where more complex influence factors are coupled. Furthermore, it can be seen that the proposed method degrades the accuracy compared with MTO, which is reflected by higher RMSE values for all types of buildings in the training and test set. This indicates that the proposed method sacrifices some accuracy in pursuit of the operation cost minimization. The results on MAE and R2 metrics are similar to those of the RMSE, which are also caused by the integration of cost considerations within the training objective of the proposed method.

In Fig. 8, we present the temperature curves of the 6-zone building on the period 12/08-14/08 of the test set. The predicted temperature data from both the proposed method and MTO exhibit a close shape and demonstrate a similar error distribution when compared with the true data. The major difference lies in the conservative nature of the temperature data generated by the proposed method, e.g., compared with MTO, the data are generally lower in the peak period and higher in the valley period. This conservativeness tends to reduce temperature violations.

TABLE II  
MODEL PERFORMANCE ON OPERATION COSTS (\$)

Buildings	Costs	Train					Test				
		RC	MTO	Proposed	vs RC	vs MTO	RC	MTO	Proposed	vs RC	vs MTO
6	Power	326.65	313.69	313.65	-4.00%	-0.01%	158.88	155.34	155.36	-2.22%	-0.01%
	Tem	57.06	82.72	46.66	-18.23%	-43.59%	48.29	62.26	38.77	-19.71%	-37.73%
	Sum	<b>383.71</b>	<b>396.41</b>	<b>360.31</b>	<b>-6.10%</b>	<b>-9.11%</b>	<b>207.17</b>	<b>217.60</b>	<b>194.13</b>	<b>-6.29%</b>	<b>-10.79%</b>
10	Power	917.80	914.33	913.84	-0.43%	-0.05%	486.46	485.29	485.49	-0.20%	0.04%
	Tem	193.11	190.54	184.78	-4.31%	-3.02%	93.29	88.88	85.46	-8.39%	-3.85%
	Sum	<b>1110.91</b>	<b>1104.87</b>	<b>1098.62</b>	<b>-1.11%</b>	<b>-0.57%</b>	<b>579.75</b>	<b>574.17</b>	<b>570.95</b>	<b>-1.52%</b>	<b>-0.56%</b>
18	Power	2973.06	2957.18	2956.89	-0.54%	-0.01%	1473.28	1466.10	1464.15	-0.62%	-0.13%
	Tem	16.16	27.75	24.75	53.16%	-10.81%	1.63	6.87	6.34	288.96%	-7.72%
	Sum	<b>2989.22</b>	<b>2984.93</b>	<b>2981.64</b>	<b>-0.25%</b>	<b>-0.11%</b>	<b>1474.91</b>	<b>1472.97</b>	<b>1470.49</b>	<b>-0.30%</b>	<b>-0.17%</b>

TABLE III  
MODEL PERFORMANCE ON ACCURACY METRICS

Buildings	Dataset	RMSE			MAE			R2		
		RC Model	MTO	Proposed	RC Model	MTO	Proposed	RC Model	MTO	Proposed
6-zone	Train	0.3189	0.2022	0.2064	0.2528	0.1542	0.1578	0.9604	0.9841	0.9834
	Test	0.3876	0.2710	0.2828	0.2948	0.1892	0.2066	0.9446	0.9729	0.9705
10-zone	Train	0.4705	0.3867	0.3928	0.3742	0.3151	0.2945	0.8125	0.8734	0.8694
	Test	0.4476	0.4294	0.4533	0.3353	0.3195	0.3252	0.8065	0.8219	0.8015
18-zone	Train	0.3770	0.2990	0.3030	0.2976	0.2241	0.2351	0.8136	0.8828	0.8796
	Test	0.3549	0.3322	0.3458	0.2906	0.2665	0.2813	0.8053	0.8293	0.8151

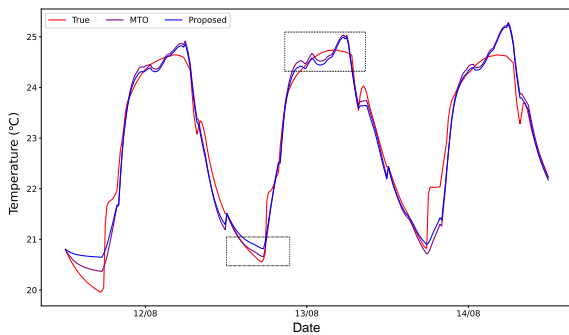


Fig. 8. Daily temperature variation of the 6-zone building.

Second, we also validate the effectiveness of the proposed penalty term in (20) to maintain the physical characteristics of the building. To that end, we compute the derivatives of the indoor temperature w.r.t. all the input features. We retrain the MTO method to ignore the added penalty terms in  $\mathcal{L}^{\text{phy}}$  for comparison. The results are presented in Fig. 9. It can be observed that the derivatives w.r.t. the indoor temperature  $\tau$  and the cooling power  $q$  are all less than 0, such that they obey the physical laws. The major difference occurs for the disturbance factors  $\mathbf{x}$ . For the proposed method, the derivatives w.r.t. the disturbance factors are all larger than 0, which properly corresponds to (20). However, for the compared method, some variables have a negative relationship with temperature variation, which violates the inherent physical constraints. This shows that the proposed penalty terms in the auxiliary loss function can effectively enforce the physical characteristics during the modeling process.

Furthermore, we compare the computational time of all

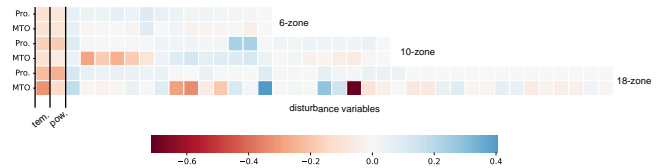


Fig. 9. Derivative of temperature w.r.t. each input feature.

methods in the model training and optimization stages. The time results are presented in Table IV. It is assumed to acquire all necessary building information to obtain the RC model in advance, so the training time of the RC model is ignored. Note that the MTO method corresponds to the pre-train stage in Algorithm 1, so the training time difference between the proposed method and MTO is the additional required time to generate the Pareto set (i.e., 29m26s in the 6-zone building, 25m52s in the 10-zone building, and 25m7s in the 18-zone building, respectively). When comparing MTO and the proposed method, it can be seen that the model training stage always requires an hour-level period, which makes it not suitable for real-time energy management applications. The required time increases with larger buildings because more input features are required to train models. Fortunately, the training stage is always conducted only once to obtain the required model, making it feasible to conduct offline training before the real-time application. Besides, it can be seen that both the RC model and the proposed model require little computational time during optimization, which shows high potential for real-time energy management in practical applications.

TABLE IV  
 COMPUTATIONAL TIME COMPARISON

Buildings	Methods	Offline Training	Optimization
6-zone	RC model	/	1.52s
	MTO	2h46m45s	1.72s
	Proposed	3h16m11s	1.93s
10-zone	RC model	/	1.73s
	MTO	4h36m34s	1.56s
	Proposed	5h2m26s	1.67s
18-zone	RC model	/	1.43s
	MTO	10h17m40s	1.64s
	Proposed	10h42m47s	1.49s

D. Performance of the Combined Gradients Method

The gradients  $g_k^*$  gathered at each iteration  $k$  of the training enable to generate a Pareto set, from which the final model is selected. Here, we analyze the performance of the proposed algorithm wherein the coordinated gradient  $g^*$  is optimized at each training epoch based on the derived  $g^{opt}$  and  $g^{phy}$ . The variations of both the objective value and the physics-informed MSE-based loss at each epoch are presented in Fig. 10.

At the beginning of the training, the model performance changes rapidly for both the objective value and the statistical accuracy. Interestingly, the model converges to a specific range where the accuracy loss closely aligns with the pre-trained model, while leading to a reduction in the objective value. The dashed boxes in the left-hand side subplots highlight the epoch of the final selected model in Algorithm 1.

Figs. 10b, 10d, and 10f show the model determination process (Step III in Algorithm 1) for the 6-zone, 10-zone, and 18-zone building, respectively. The blue point represents the pre-trained model after Step I and the red point represents the final model after Step III. The pre-trained model (epoch 0) is very accurate since it is trained with the loss function  $L^{phy}$  but the resulting costs are relatively high as the optimization problem is not considered in the training. The pink region corresponds to the preset accuracy tolerance range. During the training process, one can see that a large part of the points fall into the pink range, thus providing valuable candidate model parameters. In the 6-zone building, the generated Pareto set yields operation costs much lower than the initial black point. In the 10-zone and 18-zone buildings, some intermediate points during the training lead to higher costs than the pre-trained model but many points still fall into the pink region. This indicates that the proposed algorithm can reach Pareto points with lower operation costs (while keeping a good accuracy) by coordinating gradients adaptively.

To analyze the effectiveness of the proposed algorithm, we compare it with the regular gradient combination with fixed weights, i.e.,  $g^* = g^{opt} + \omega \cdot g^{phy}$ , where  $\omega$  is selected from the set  $\{0, 1, 2, 3, 4, 5\}$ . The operation costs of each case are presented in Fig. 11, where the y-axis is the relative cost difference compared with the proposed method, i.e., a positive value means that the proposed method outperforms the regular approach. It can be found that the gradient combination with fixed weights can achieve lower costs when  $\omega = [0, 1, 2, 3]$  but the costs increase beyond the proposed method with higher

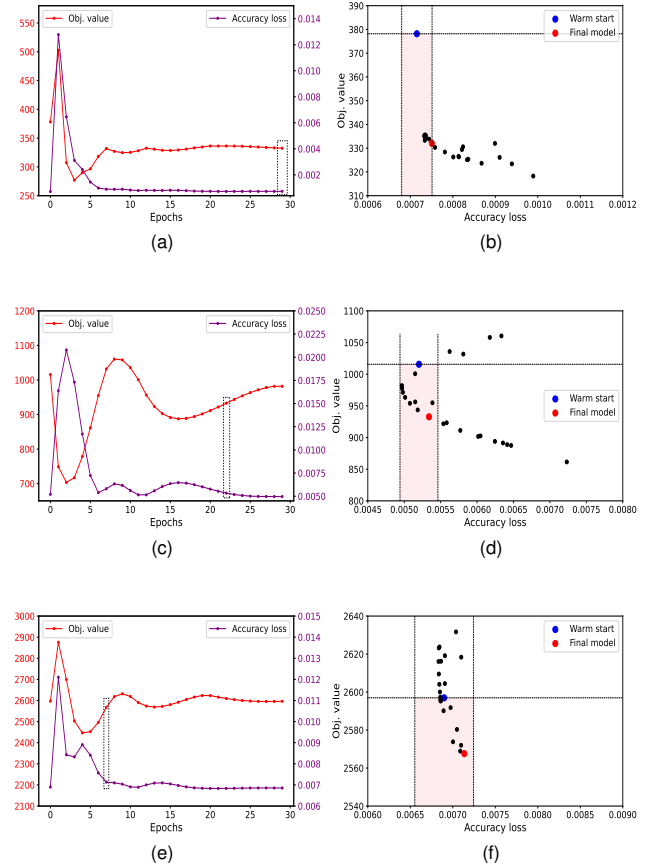


Fig. 10. Training process based on the proposed algorithm; (a), (c), and (e) show iterative variations of both objective costs and accuracy losses; (b), (d), and (f) show Pareto set for the determined model; (a)-(b), (c)-(d), and (e)-(f) are from 6-zone, 10-zone, and 18-zone building, respectively.

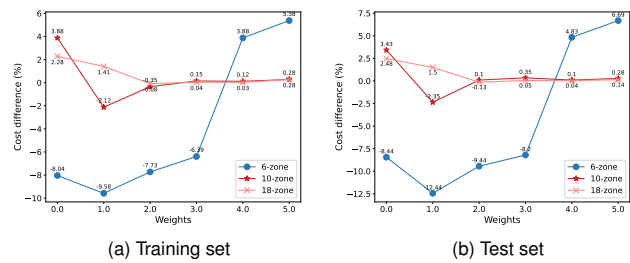


Fig. 11. Comparison of operation costs of different cases on training and test sets.

weighting values. As for the studied 10-zone and 18-zone cases, the proposed method leads to the lowest costs. The cost differences remain stable regardless of the weight  $\omega$ . For the 6-zone building, the decreasing weights can effectively reduce the optimization costs, but it should be noted that, in practice, it would be very difficult to find the optimal  $\omega$ -value in an ex-ante fashion. Overall, these results indicate that the fixed weight-based method, even if the optimal weight  $\omega$  could be known in advance, can not always guarantee cost reduction in the downstream optimization problem.

TABLE V  
MODEL PERFORMANCE OF 67- AND 90-ZONE BUILDINGS

Buildings	Dataset	Costs			RMSE			MAE			R2		
		MTO	Proposed	vs MTO	MTO	Proposed	vs MTO	MTO	Proposed	vs MTO	MTO	Proposed	vs MTO
67-zone	Train	2692.86	2683.09	-0.36%	0.2656	0.2710	2.03%	0.2011	0.2051	1.99%	0.9695	0.9682	-0.13%
	Test	1352.95	1344.03	-0.66%	0.3779	0.3717	-1.64%	0.2896	0.2842	-1.87%	0.9384	0.9404	0.21%
90-zone	Train	3549.62	3510.41	-1.11%	0.3587	0.3719	3.68%	0.2728	0.2989	9.57%	0.8690	0.8591	-1.14%
	Test	1390.30	1386.95	-0.24%	0.4496	0.3649	-18.84%	0.3359	0.2817	-16.14%	0.7889	0.8610	9.14%

### E. Scalability and Robustness Analysis

On the basis of existing building cases, we further verify the scalability and robustness of the proposed method in buildings with more complex structures. Here, a hotel prototype with 67 zones and an apartment prototype with 90 zones from DOE are simulated. To further demonstrate the performance difference between MTO and the proposed method, we still compare them in 67-zone and 90-zone building cases. Firstly, the performances of optimization costs and modeling accuracy are comprehensively evaluated. The results are presented in Table V. It can be seen that the proposed method can still reduce optimization costs effectively compared with the MTO method in the two cases. Similar accuracy performance can be found in that the proposed method sacrifices some accuracy in pursuit of operation cost minimization during the training process. However, the proposed method can achieve lower errors in the test set than the MTO method. It shows a potential advantage of the proposed method to mitigate over-fitting risks in MTO. The overly accurate training performance happens in the model after the pre-train stage (i.e., the MTO model) in Algorithm 1. Then the proposed method can improve this situation by modifying the loss function during the fine-tuning stage, where the over-fitting risks can be alleviated by optimizing parameter update directions.

Furthermore, to make our case study more valuable to the actual data-driven situations, we set different data missing rates to simulate the limited data measurement scenarios in the real world. Specifically, we assume various missing rates (i.e., 0.1-0.5) of input features involving both power  $q$  and disturbance variables  $x$ . We then train models with corresponding input data and simulate the performance in both optimization costs and modeling accuracy. The results of optimization costs with the increased missing rates are shown in Fig. 12. It can be found that the optimization costs are merely influenced by various data missing settings in both MTO and the proposed method. Furthermore, we compare the modeling accuracy performances in Fig. 13, where RMSE metrics are adopted for evaluation. Similar to cost results, it can be found that the model is robust to various missing rates with similar accuracy performance. The increased missing rates will enlarge the RMSE errors slightly but still be acceptable in training and test sets.

### F. Implementation Analysis

Based on the above case simulation results, this subsection further explains how to incorporate the novel training process into the practical Building Energy Systems (BEMSs) for building temperature control [39]. Compared with the existing

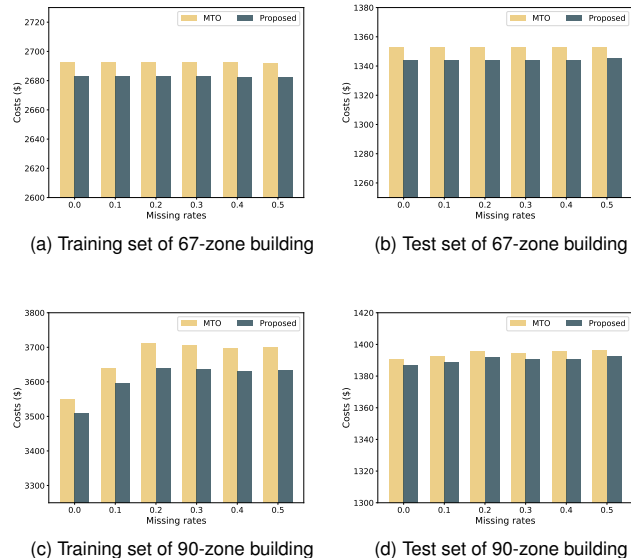


Fig. 12. Optimization costs with increased missing rates.

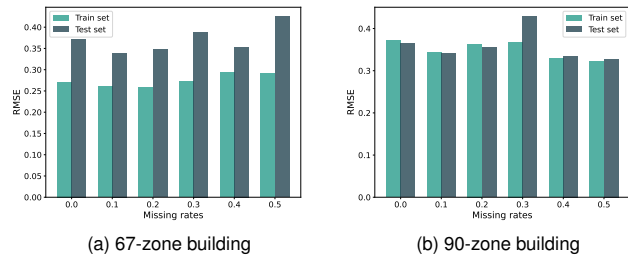


Fig. 13. RMSE performance with increased missing rates.

approaches (e.g., optimal control and reinforcement learning-based energy management problems), the proposed work incorporates the modeling process into the decision-making stage by designing decision-oriented loss functions for model training. The major advantage is that it can achieve lower decision costs in practical applications by training a more cost-aware model. However, as shown in Subsection V.C, the disadvantage mainly refers to the higher computational burden of training caused by solving the downstream optimization problem during each iteration.

To make the proposed work more efficient in practical application, we introduce a feasible application mechanism in BEMSs, which is shown in Fig. 14. Specifically, the implementation procedure involves both offline model training and online temperature control sectors. In the offline sector,

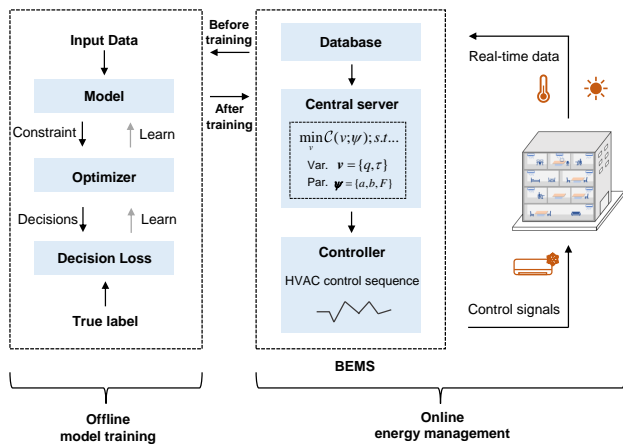


Fig. 14. Implementation details of the proposed work in BEMSs.

relevant data are collected as input for the model training process. The downstream optimization task for model training corresponds to the actual control purpose in the central server in BEMSs. The offline sector can avoid the high computational time required during the model parameter update of neural networks. After the model training process, the obtained model is incorporated into the central server in BEMSs, which is regarded as the reference model for building energy management (e.g., state-space function in optimal control methods). Note that our proposed method highlights the modeling problem of thermal dynamics, where the complex HVAC control actions are simplified as cooling power signals.

## VI. CONCLUSIONS

This paper presents a novel approach for learning the thermal dynamics of buildings. We depart from traditional methods that are trained to minimize statistical loss functions. To that end, we aim to propose a new model training strategy oriented by the objective of the downstream optimization process. This objective is then enhanced with an auxiliary accuracy metric to ensure that the learned model complies with known physical constraints. The proposed method achieves lower operation costs than the traditional accuracy-oriented modeling methods for various types of buildings. The reduction in costs primarily stems from a decrease in violations of temperature constraints, accompanied by additional gains from improved power consumption schedules. This tends to demonstrate that the proposed model has properly learned to avoid zones leading to expensive costs.

In future research, the proposed decision-oriented strategy can be extended to more diverse scenarios: (1) conduct thermal dynamics modeling method under more complex application scenarios (e.g., by accounting for frequency regulation, or other market services) in order to explore the ability of the method to capture more complex constraints; (2) incorporate the decision-oriented strategy with model-free method (e.g., Reinforcement learning) to train cost-aware agents for real-time temperature control; (3) consider both the uncertain model parameters and forecasting disturbance terms jointly in the building temperature control problem.

## REFERENCES

- [1] R. Newell, D. Raimi, S. Villanueva, B. Prest *et al.*, "Global energy outlook 2021: pathways from Paris," *Resources for the Future*, vol. 8, 2021.
- [2] UN Environment Programme, "2022 Global Status Report for Buildings and Construction," [Online], <https://globalabc.org/our-work/tracking-progress-global-status-report>.
- [3] R. Wang and X. Zhai, *Handbook of energy systems in green buildings*. Springer, 2018, vol. 160.
- [4] Y. Yao and D. K. Shekhar, "State of the art review on model predictive control (MPC) in heating ventilation and air-conditioning (HVAC) field," *Building and Environment*, vol. 200, p. 107952, 2021.
- [5] V. Harish and A. Kumar, "A review on modeling and simulation of building energy systems," *Renewable and sustainable energy reviews*, vol. 56, pp. 1272–1292, 2016.
- [6] D. B. Crawley, L. K. Lawrie, C. O. Pedersen, and F. C. Winkelmann, "Energy plus: energy simulation program," *ASHRAE journal*, vol. 42, no. 4, pp. 49–56, 2000.
- [7] "TRNSYS: Transient System Simulation Tool," [Online], <http://www.trnsys.com/>.
- [8] Z. Wang and Y. Chen, "Data-driven modeling of building thermal dynamics: Methodology and state of the art," *Energy and Buildings*, vol. 203, p. 109405, 2019.
- [9] S. Lu, W. Gu, S. Ding, S. Yao, H. Lu, and X. Yuan, "Data-driven aggregate thermal dynamic model for buildings: A regression approach," *IEEE Transactions on Smart Grid*, vol. 13, no. 1, pp. 227–242, 2021.
- [10] Y.-J. Kim, "A supervised-learning-based strategy for optimal demand response of an HVAC system in a multi-zone office building," *IEEE Transactions on Smart Grid*, vol. 11, no. 5, pp. 4212–4226, 2020.
- [11] Y. Li, Z. O'Neill, L. Zhang, J. Chen, P. Im, and J. DeGraw, "Grey-box modeling and application for building energy simulations-A critical review," *Renewable and Sustainable Energy Reviews*, vol. 146, p. 111174, 2021.
- [12] M. K. Muthalib and C. O. Nwankpa, "Physically-based building load model for electric grid operation and planning," *IEEE Transactions on Smart Grid*, vol. 8, no. 1, pp. 169–177, 2016.
- [13] Z. Wei, F. Ren, Y. Zhu, B. Yue, Y. Ding, C. Zheng, B. Li, and X. Zhai, "Data-driven two-step identification of building thermal characteristics: A case study of office building," *Applied Energy*, vol. 326, p. 119949, 2022.
- [14] X. Cui, S. Liu, G. Ruan, and Y. Wang, "Data-driven aggregation of thermal dynamics within building virtual power plants," *Applied Energy*, vol. 353, p. 122126, 2024.
- [15] G. E. Karniadakis, I. G. Kevrekidis, L. Lu, P. Perdikaris, S. Wang, and L. Yang, "Physics-informed machine learning," *Nature Reviews Physics*, vol. 3, no. 6, pp. 422–440, 2021.
- [16] G. Gokhale, B. Claessens, and C. Develder, "Physics informed neural networks for control oriented thermal modeling of buildings," *Applied Energy*, vol. 314, p. 118852, 2022.
- [17] J. Drgoňa, A. R. Tuor, V. Chandan, and D. L. Vrabie, "Physics-constrained deep learning of multi-zone building thermal dynamics," *Energy and Buildings*, vol. 243, p. 110992, 2021.
- [18] L. Di Natale, B. Svetozarevic, P. Heer, and C. N. Jones, "Physically consistent neural networks for building thermal modeling: theory and analysis," *Applied Energy*, vol. 325, p. 119806, 2022.
- [19] T. Xiao and F. You, "Building thermal modeling and model predictive control with physically consistent deep learning for decarbonization and energy optimization," *Applied Energy*, vol. 342, p. 121165, 2023.
- [20] J. Zhang, Y. Wang, and G. Hug, "Cost-oriented load forecasting," *Electric Power Systems Research*, vol. 205, p. 107723, 2022.
- [21] J. Han, L. Yan, and Z. Li, "A task-based day-ahead load forecasting model for stochastic economic dispatch," *IEEE Transactions on Power Systems*, vol. 36, no. 6, pp. 5294–5304, 2021.
- [22] G. Li and H.-D. Chiang, "Toward cost-oriented forecasting of wind power generation," *IEEE Transactions on Smart Grid*, vol. 9, no. 4, pp. 2508–2517, 2016.
- [23] I. Khabibrakhmanov, S. Lu, H. F. Hamann, and K. Warren, "On the usefulness of solar energy forecasting in the presence of asymmetric costs of errors," *IBM Journal of Research and Development*, vol. 60, no. 1, pp. 7–1, 2016.
- [24] R. T. Chen, Y. Rubanova, J. Bettencourt, and D. K. Duvenaud, "Neural ordinary differential equations," *Advances in neural information processing systems*, vol. 31, 2018.
- [25] A. Tuor, J. Drgoňa, and D. Vrabie, "Constrained neural ordinary differential equations with stability guarantees," *arXiv preprint arXiv:2004.10883*, 2020.

- [26] M. Zakwan, L. Di Natale, B. Svetozarevic, P. Heer, C. N. Jones, and G. F. Trecate, "Physically consistent neural odes for learning multi-physics systems," *arXiv preprint arXiv:2211.06130*, 2022.
- [27] Y. Chen, Y. Shi, and B. Zhang, "Optimal control via neural networks: A convex approach," *arXiv preprint arXiv:1805.11835*, 2018.
- [28] R. Fernández-Blanco, J. M. Morales, and S. Pineda, "Forecasting the price-response of a pool of buildings via homothetic inverse optimization," *Applied Energy*, vol. 290, p. 116791, 2021.
- [29] B. Amos and J. Z. Kolter, "Optnet: Differentiable optimization as a layer in neural networks," in *International Conference on Machine Learning*. PMLR, 2017, pp. 136–145.
- [30] S. G. Krantz and H. R. Parks, *The implicit function theorem: history, theory, and applications*. Springer Science & Business Media, 2002.
- [31] J. Mandi, J. Kotary, S. Berden, M. Mulamba, V. Bucarey, T. Guns, and F. Fioretto, "Decision-focused learning: Foundations, state of the art, benchmark and future opportunities," *arXiv preprint arXiv:2307.13565*, 2023.
- [32] B. Liu, X. Liu, X. Jin, P. Stone, and Q. Liu, "Conflict-averse gradient descent for multi-task learning," *Advances in Neural Information Processing Systems*, vol. 34, pp. 18 878–18 890, 2021.
- [33] "Energyplus," [Online], <https://energyplus.net/>.
- [34] Y. Xu and C. Singh, "Adequacy and economy analysis of distribution systems integrated with electric energy storage and renewable energy resources," *IEEE Transactions on Power Systems*, vol. 27, no. 4, pp. 2332–2341, 2012.
- [35] Supplementary materials, "Dataset settings of building operation in case study," [Online], <https://github.com/cuixueyuan/Related-data-for-optimization-oriented-modeling->.
- [36] A. Paszke, S. Gross, S. Chintala, G. Chanan, E. Yang, Z. DeVito, Z. Lin, A. Desmaison, L. Antiga, and A. Lerer, "Automatic differentiation in pytorch," 2017.
- [37] R. T. Q. Chen, "torchdiffeq," 2018. [Online]. Available: <https://github.com/rtqichen/torchdiffeq>
- [38] A. Agrawal, B. Amos, S. Barratt, S. Boyd, S. Diamond, and Z. Kolter, "Differentiable Convex Optimization Layers," in *Advances in Neural Information Processing Systems*, 2019.
- [39] M. Manic, D. Wijayasekara, K. Amarasinghe, and J. J. Rodriguez-Andina, "Building energy management systems: The age of intelligent and adaptive buildings," *IEEE Industrial Electronics Magazine*, vol. 10, no. 1, pp. 25–39, 2016.



**Xueyuan Cui** received the B.E. and M.S. degrees from Zhejiang University, Hangzhou, China, in June 2019 and March 2022, respectively, both in electrical engineering. He is currently a Ph.D. student with the Department of Electrical and Electronic Engineering, The University of Hong Kong. His research interests include data-driven building energy management.



**Jean-François Toubeau** received the degree in civil electrical engineering, and the Ph.D. degree in electrical engineering, from University of Mons (Belgium) in 2013 and 2018, respectively. He is currently a full-time senior researcher within the "Power Systems and Markets Research Group" at University of Mons. His research mainly focuses on bridging the gap between machine learning and decision-making in modern power systems.



**François Vallée** received the degree in civil electrical engineering and the Ph.D. degree in electrical engineering from the Faculty of Engineering, University of Mons, Belgium, in 2003 and 2009, respectively. He is currently a Professor and leader of the "Power Systems and Markets Research Group" at University of Mons. His Ph.D. work has been awarded by the SRBE/KBVE Robert Sinave Award in 2010. His research interests include PV and wind generation modeling for electrical system reliability studies in presence of dispersed generation.



**Yi Wang** received the B.S. degree from Huazhong University of Science and Technology in June 2014, and the Ph.D. degree from Tsinghua University in January 2019. He was a visiting student with the University of Washington from March 2017 to April 2018. He served as a Postdoctoral Researcher in the Power Systems Laboratory, ETH Zurich from February 2019 to August 2021.

He is currently an Assistant Professor with the Department of Electrical and Electronic Engineering, The University of Hong Kong. His research interests

include data analytics in smart grids, energy forecasting, multi-energy systems, Internet-of-things, cyber-physical-social energy systems.